Chemistry Europe
European Chemical Societies Publishing

Special Issue

On the Hydrogen Oxalate Binding Motifs onto Dinuclear Cu and Ag Metal Phosphine Complexes

Björn Kwasigroch,[a] Thien Khuu,[b] Evan H. Perez,[b] Joanna K. Denton,[b] Erik K. Schneider,[c] Annika Straßner,[a] Marvin Theisen,[a] Sebastian V. Kruppa,[a] Patrick Weis,[c] Manfred M. Kappes,[c, e] Christoph Riehn,[a, d] Mark A. Johnson,[b] and Gereon Niedner-Schatteburg*[a, d]

Abstract: We report the binding geometries of the isomers that are formed when the hydrogen oxalate ($(CO_2)_2H=HOx$) anion attaches to dinuclear coinage metal phosphine complexes of the form $[M_1M_2dcpm_2(HOx)]^+$ with M = Cu, Ag and dcpm = bis(dicyclohexylphosphino)methane, abbreviated **[MM]$^+$**. These structures are established by comparison of isomer-selective experimental vibrational band patterns displayed by the cryogenically cooled and N_2-tagged cations with DFT calculations of the predicted spectra for various local minima. Two isomeric classes are identified that feature either attachment of the carboxylate oxygen atoms to the two metal centers (end-on docking) or attachment of oxygen atoms on different carbon atoms asymmetrically to the metal ions (side-on docking). Within each class, there are additional isomeric variations according to the orientation of the OH group. This behavior indicates that HOx undergoes strong and directional coordination to **[CuCu]$^+$** but adopts a more flexible coordination to **[AgAg]$^+$**. Infrared spectra of the bare ions, fragmentation thresholds and ion mobility measurements are reported to explore the behaviors of the complexes at ambient temperature.

Introduction

CO_2 capture and storage are mandatory in order to check climate change and allow for a sustainable worldwide economy going forward. There are two routes operational in nature: photosynthetic CO_2 fixation by RuBisCO with the cofactor Mg^{2+} and conversion of oceanic CO_2 to carbonic acid with ultimate fixation via formation of bicarbonate through calcifying organisms.[1] Synthetic chemists have found alternative routes, some of which are based on dinuclear Cu complexes.[2] More specifically, DFT calculations indicate that CO_2 stabilization arises through association of mononuclear complexes into a pair of oxalate bridged dinuclear complexes,[3] and these catalytic cycles end with the expulsion of oxalate products, leaving behind dissociated mononuclear remainders.[2] Such bridging oxalate dinuclear coinage metal complexes with phosphine ligands are important in industrial applications, such as precursors for Chemical Vapor Deposition (CVD) in copper/silver coating production.[4]

In this report, we characterize the oxalate binding motifs to two dinuclear complexes by analyzing the vibrational spectra of the isolated ions that are cryogenically cooled in the gas-phase.[5] These complexes are based on the stable dinuclear d^{10} metal compounds formed by chelation of Cu^+ and Ag^+ with the phosphine ligand bis(dicyclohexylphosphino)methane (dcpm). Attachment of the $HC_2O_4^-$ anion (hereafter denoted HOx) to the dicationic dimetallic compounds, $[M_1M_2dcpm_2]^{2+}$ (M = Cu, Ag; dcpm = bis(dicyclohexylphosphino)methane), yields the non-covalently bound structure indicated schematically in Scheme 1. Hereafter, we denote these complexes (including all ligands) as **[CuCu]$^+$** or **[AgAg]$^+$**. Analogous motifs have found applications as organic light emitting diodes (OLEDs), photocatalysts,[6] catalyst model systems,[7] and have been used to explore metallophilic interactions.[8] For example, C–C coupling photoreactions arise from $[Au_2(\mu\text{-dppm})_2]^{2+}$ and

[a] B. Kwasigroch, A. Straßner, M. Theisen, Dr. S. V. Kruppa, Dr. C. Riehn, Prof. Dr. G. Niedner-Schatteburg
Department of Chemistry, Technische Universität Kaiserslautern (TUK)
Erwin-Schrödinger-Str. 52, 67663 Kaiserslautern (Germany)
E-mail: gns@chemie.uni-kl.de

[b] T. Khuu, E. H. Perez, Dr. J. K. Denton, Prof. M. A. Johnson
Sterling Chemistry Laboratory, Yale University
225 Prospect Str., New Haven, Connecticut 06520 (USA)

[c] E. K. Schneider, Dr. P. Weis, Prof. Dr. M. M. Kappes
Institute of Physical Chemistry, Karlsruhe Institute of Technology (KIT)
Fritz-Haber Weg 2, 76131Karlsruhe (Germany)

[d] Dr. C. Riehn, Prof. Dr. G. Niedner-Schatteburg
Research Center OPTIMAS, Erwin-Schrödinger Str. 46
67663 Kaiserslautern (Germany)

[e] Prof. Dr. M. M. Kappes
Institute for Nanotechnology, Karlsruhe Institute of Technology (KIT)
Hermann-von-Helmholtz-Platz 1, 76344 Eggenstein-Leopoldshafen (Germany)

Supporting information for this article is available on the WWW under https://doi.org/10.1002/chem.202102768

Special Issue This manuscript is part of a Special Issue "Cooperative effects in heterometallic complexes".

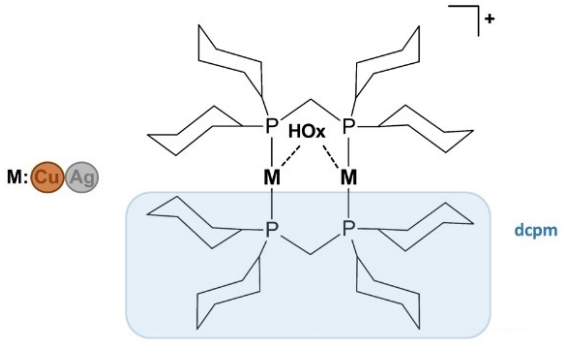

Scheme 1. The investigated binuclear coinage metal phosphine complexes with hydrogen oxalate (HOx) adduct.

$[Cu_2(\mu\text{-dppm})_2(MeCN)_4]^{2+}$ complexes (where μ indicates bridging, dppm = bis(diphenylphosphino)methane) that are active in catalytic amounts.[9] Spectroscopic characterization of related compounds recovered structural evidence for some argentophilicity,[10] which is in line with related studies on metallophilicity.[11]

The metal centers in the Scheme 1 structure are nominally present in the +1 charge state, thus providing docking sites for complexation with the oxygen atoms of HOx. Two distinct classes of binding were recovered by our DFT calculations (see below) with the key structural elements indicated in Scheme 2. It is evident that the HOx anion presents a versatile scaffold upon binding to metal centers: it can be attached in an "end-on", bidentate arrangement (eb) involving attachment to the metals with the oxygen atoms on the carboxylate group, or "side-on" in which both metals interact with one of the HOx oxygen atoms, denoted (sμ or smμ). In each of these motifs, the H-atom can either bridge between proximal O atoms (denoted Hb) or point away as a free OH group (Hf). As we discuss further below, the end-on motif is predicted to occur with quasi-symmetrical attachment of the $-CO_2^-$ group to the two metal ions or with asymmetrical binding such that one oxygen atom is closer to both metal atoms while the other is bound to one of the metal centers. The side-on docking motif also features interaction of the oxygen atom from the $-CO_2^-$ moiety to both metals, but with the acid C=O group bound to only one of the metal ions. It is evident that this variation in binding motifs thus reveals the delicate balance of forces at play as the excess electron density and H-atom location adjust to maximize the overall interaction. Cryogenic IR spectroscopy has proven to be a useful method for identifying such structural motifs via analysis of the spectral evolution of the CO and OH vibrational fundamentals of the bare ion upon attachment to the metal ion centers with DFT calculations.[12] HOx has six vibrational normal modes with fundamentals in the IR range that are accessible with contemporary OPO/A laser technology. Frequency shifts and IR intensities of these vibrational modes are predicted to vary according to the coordination motifs (Scheme 2) and the identities of the coordinating metals, as we discuss further in the results and discussion part. Several values for the various groups are included at the bottom of Scheme 2.

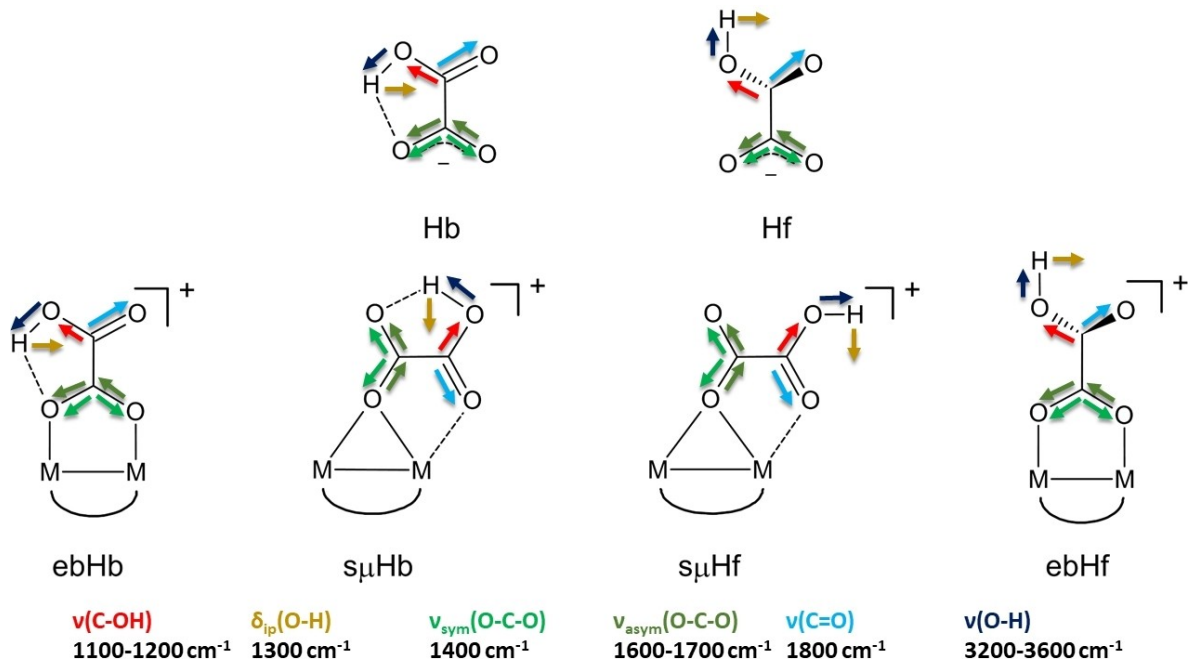

Scheme 2. Possible binding motifs of free hydrogen oxalate anion (top, two isomers) and of coordinated hydrogen oxalate anion (middle, M(I), four examples for possible binding motif). Six "fingerprinting" vibration modes (1000–4000 cm^{-1}) are indicated. Isomers are coded for their structures as follows: e: end-on, s: side-on, b: bidentate, μ: one O-atom coordinates between two metals, Hf: free OH, Hb: bound OH.

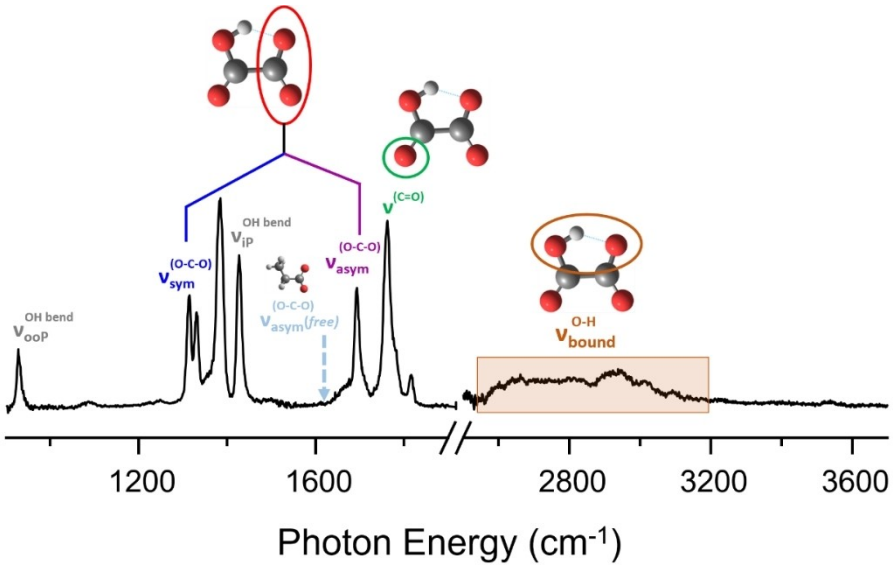

Figure 1. Summary of the vibrational spectrum and band assignments in H_2-tagged HOx. The blue $\nu_{sym}^{(O-C-O)}$ and purple $\nu_{asym}^{(O-C-O)}$ represent the symmetric and asymmetric stretches of the oxalate anion nominal $-CO_2^-$, respectively, with the dashed vertical arrow indicating the $\nu_{asym}^{(O-C-O)}$ fundamental of the free carboxylate group on propionate for reference.[12] The diffuse band highlighted in the orange box (ν_{bound}^{O-H}) is derived from the OH stretch of the oxalate anion, with a representative structure shown in the insets. The grey labels $\nu_{ooP}^{OH\ bend}$ and $\nu_{iP}^{OH\ bend}$ are the out-of-plane and in-plane OH bend, respectively. The green label $\nu^{(C=O)}$ indicates the carbonyl stretch of the oxalate anion. The spectrum is adapted with permission from Ref. [19] Copyright 2015, American Chemical Society.

Experimental Methods

Sample preparation and IR photodissociation spectroscopy

Samples of $[M_1M_2(dcpm)_2](PF6)_2$ (M = Cu, Ag) (synthesized according to Ref. [10]) and oxalic acid (98%, Sigma-Aldrich) were dissolved and diluted in methanol (VWR, HPLC grade, $c = 10^{-6}$ mol/l, stoichiometric ratio 10:1). The hydrogen oxalate complex cations were transferred into the gas phase by electrospray ionization (ESI). The one- and two-color cryo IR-PD and IR-IR experiments (with OPO/A laser system, LaserVision; pumped with a pulsed 10 Hz injection seeded Nd^{3+}: YAG laser, SL-EX, Continuum) were carried out at Yale University by a previously described setup.[13] Briefly, the species in question are cooled and N_2-tagged in a temperature-controlled cryostat to ~40 K. They are then intercepted by a scanning IR bleach/pump beam, which excites resonant transitions producing untagged fragment ions, which are separated from the remaining intact parent species (i.e., the tagged ions) by time-of-flight using a reflectron. The tagged parent ions are then intersected by a fixed frequency IR probe beam. This probe beam is set to the frequency of a transition due to one of the isomers, and its photofragment yield provides a measurement of the population of this isomer. This signal is then modulated by the scanning bleach/pump laser when it depletes the probed isomer. Due to the low ion yield observed for this experiment, this data was collected point-by-point, using a 10 Hz probe laser to average the fragmentation yield difference between on and off states of the 5 Hz bleach laser for 2000–11300 cycles (IR-IR two color hole burning experiments). The infrared multiple photon dissociation (IR-MPD) measurements were carried out at TU Kaiserslautern using a modified quadrupole ion trap (Paul trap) mass spectrometer (QIT MS, Amazon SL, Bruker Daltonics). This instrument was also used to carry out ESI mass spectrometry (ESI-MS) and collision-induced dissociation (CID). Details of the CID measurements are included in the Supporting Information.

The infrared multiple photon dissociation (IR-MPD) experiments at TUK (Technical University of Kaiserslautern) were carried out by irradiating mass-selected ions in the Paul trap with one or more laser pulses from a KTP/KTA optical parametric oscillator/amplifier (OPO/A, LaserVision) system pumped with a pulsed 10 Hz injection seeded Nd^{3+}: YAG laser (PL8000, Continuum), when stored within the quadrupole ion trap. The instrument and laser system settings were described before.[14]

Ion mobility studies at KIT

TIMS experiments at KIT (Karlsruhe Institute of Technology) took place by using a Bruker timsTOF mass spectrometer. The capillary voltage was 3.5 kV, the nebulizer pressure 0.2 bar, dry gas flow was 3 l/min at a temperature of 200 °C. To record spectra by trapped ion mobility spectrometry (TIMS), the ions are held by an electric field while exposed to a constant N_2 flow across the TIMS-tunnel due to a small pressure difference between its entrance and the exit. The ions are eluted by slowly decreasing the electric field. The ion mobility data were determined by both the standard "survey" and the high-resolution mode ("ultra" or "custom" with 500 ms ramp time and $1/K_0$ interval width of 0.05 Vs/cm^2) of the timsTOF instrument. Under these conditions, the instrumental resolving power (in terms of collision cross section CCS: CCS/ΔCCS) was typically above 200.

DFT modelling

DFT-calculations were conducted to identify stable and likely structures as well as interconversion pathways between the local minima. The level of theory was the exchange correlation functional PBE0 with basis set/effective core potential def2TZVP.[15] The software package Gaussian 16 was used.[16] Stable structures were verified as stable minima by absence of imaginary modes. Zero-point energy/correction, enthalpy and free Gibbs enthalpy were

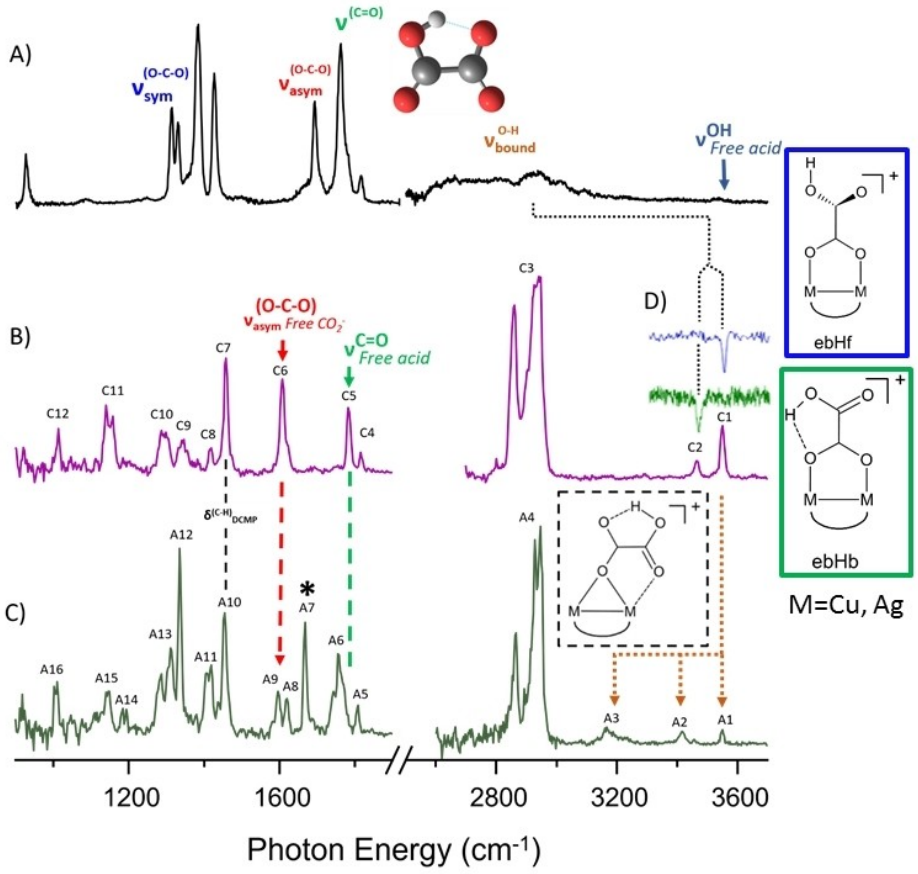

Figure 2. Evolution of bands assigned to HOx upon complexation to $[M_2dcpm_2]^{2+}$ (M = Cu, Ag). A) Vibrational spectrum of H_2-tagged HOx, reproduced and modified from reference with permission.[19] The labels and color scheme are the same as in Figure 1. B–C) N_2-tagged vibrational spectra of **[CuCu]**$^+$ and **[AgAg]**$^+$, with peak labels from C1–C12 and A1–A16, respectively, for ease of reference in text. The assignments for these peaks are shown in Tables 1 and 2, see below. The * on A7 in C) indicates the blueshifted $\nu_{asym}^{(O-C-O)}$ of the **[AgAg]**$^+$ complex with the HOx adduct bound in a side-on fashion (sμ or smμ). The sμHb binding motif is displayed inset in a dashed square. D) IR-IR hole burning spectra probing at C1 (blue, 3551 cm^{-1}) and C2 (green, 3467 cm^{-1}) positions. The dip spectra separate the heterogeneous spectrum to reveal patterns of two isomers, both with the HOx adduct bound in an end-on fashion (eb), but one with a free-OH (Hf) and the other with a bound-OH (Hb) (blue and green traces, respectively). The ebHf and ebHb binding motifs are shown inset, boxed in blue and green rectangles. Vertical dashed lines show the spectral shifts of various HOx vibrational transitions upon complexation with $[M_2dcpm_2]^{2+}$.

calculated at 298.15 K and 1.0 Atm. Transition state calculations took place by relaxed potential energy surface scans, by the QST3 routine and by presence of a single imaginary mode via frequencies calculation.[17] DFT vibration scaling were chosen as 0.961 (1000–2200 cm^{-1}) and 0.946 (2600–3800 cm^{-1}) to match with the most intense IR-PD/IR-MPD bands (e.g., $\nu(C{-}H)_{dcpm}$ at 2861/2939 cm^{-1}). The PBE0 functional was found before to provide for satisfactory results in good agreement with QCISD(T) and CCSD(T) calculated energies in the case of small transition metal systems.[18]

Results and Discussion

Structure and vibrational band assignments for H_2-tagged Hox

The vibrational spectra and structures of the isolated HOx and DOx anions have been reported earlier,[19] and occur with the bridging H-bonded arrangement depicted in the inset at the top of Figure 1. The proton is located closer to one of the oxygen atoms in a planar, double-minimum structure in which the resulting strained H-bond tethers the two carboxylate groups together. The key features in the cold ion spectrum that reflect this structure are the pattern of sharp C=O stretching fundamentals in the fingerprint region and the very diffuse, red-shifted envelope (ν_{bound}^{O-H}) associated with the OH stretching vibration centered around 2800 cm^{-1}. The C=O stretches fall mid-way between those expected for independent $-CO_2^-$ and COOH groups, signaling asymmetrical accommodation of the proton. Specifically, the band associated mostly with the asymmetric stretch of the CO_2^- moiety lies above that of the in the propionate anion $\left(\nu_{asym}^{(O-C-O)}\right)$, indicated by a vertical dashed arrow in Figure 1. The origin of the very diffuse ν_{bound}^{O-H} band near 2800 cm^{-1} has been analyzed in the context of a vibrationally adiabatic picture where vibrational excitation explores configurations in which the proton migrates toward the oxygen on the nominal $-CO_2^-$ carboxylate moiety.

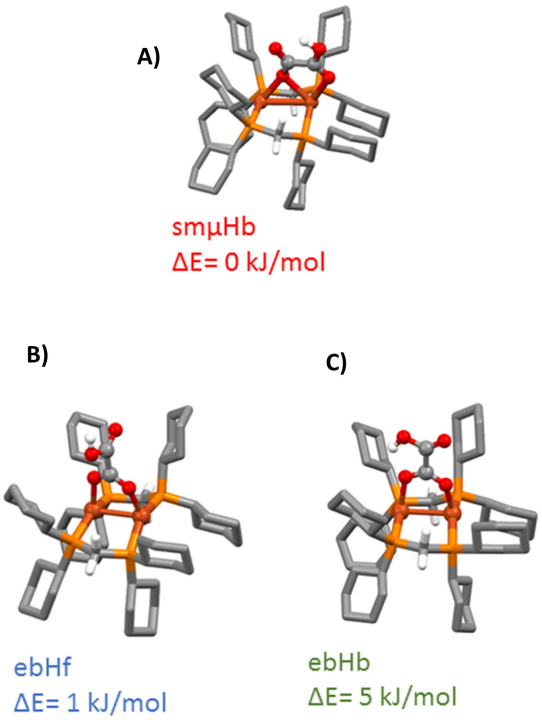

Figure 3. Lowest three structures calculated for the **[CuCu]**$^+$ complex. Atoms are coded by color (brown for Cu, orange for P, red for O, grey for C, white for H); isomers are coded for their structures as follows: e: end-on, s: side-on, b: bidentate, m: monodentate, μ: one O-atom coordinates between two metal, Hf: free OH, Hb: bonded OH. For a better overview, H atoms of the cyclohexyl groups are omitted. Relative energies are given for each isomer. More isomers are shown in Figure S1. Level of theory: PBE0/def2TZVP.

Evolution of the HOx spectral features in the vibrational spectra of the N_2-tagged [CuCu]$^+$ and [AgAg]$^+$ complexes

Figure 2 presents a comparison of the bare HOx spectrum in trace A with those of the **[CuCu]**$^+$ and **[AgAg]**$^+$ complexes in B and C, respectively. The strong features near 2900–3000 cm^{-1} (C3 and A4) are expected for the CH stretching modes of the dcpm ligand as are those (C7 and A10) its associated bending fundamentals near 1500 cm^{-1}. The sharper features (C1, C2, A1, A2, A3) above 3100 cm^{-1}, on the other hand are not expected from the scaffold, but are typical for OH stretching motions. As such, the dramatic blue-shift of the diffuse OH oscillator strength upon HOx complexation to the dimetallic scaffold signals localization of the H atom onto one of the oxygen atoms. In fact, the highest energy feature is present in both systems (C1, A1) and is very close to the OH fundamental in an HOx free acid –COOH group at 3565 cm^{-1}.[20] Similarly, the bands in the fingerprint region above 1500 cm^{-1} are unique to the C=O stretching modes, and the C=O stretch associated with the -COOH group occurs highest in energy, appearing at 1823 cm^{-1} in the bare acid (green arrow labeled $\nu^{C=O}_{Free\ acid}$ in Figure 2B).[19]

The band pattern displayed by the **[CuCu]**$^+$ complex is clearly simpler than that found in the **[AgAg]**$^+$ system such that the **[CuCu]**$^+$ band pattern is preserved in the **[AgAg]**$^+$ spectrum but is now embedded in a more complex set of transitions. This suggests that multiple isomers are likely in play, and we therefore first consider the structural implications encoded in the locations of the OH and CO bands in the simpler **[CuCu]**$^+$ spectrum. For example, the fact that the C=O and OH spectral signatures of an intact –COOH group are present in the **[CuCu]**$^+$ spectrum suggests that it adopts an end-on docking motif with the dimetal center. This, in turn, implies that the C6 peak near 1600 cm^{-1} arises from the O–C–O asymmetric stretching mode of the carboxylate group attached to the metals, and that band indeed redshifts very close to the location of the CO_2 asymmetric C–O stretching mode in the free d_5-propionate ion (red arrow in Figure 2B). We compare with the d_5-propionate carboxylate here because the deuterium isotopologue suppresses activity of the CH bending modes in the region of the C=O stretches.[12a] Thus, empirical analysis of the band positions strongly suggests that the ebHf isomer is the dominant species present in the **[CuCu]**$^+$ complex.

Calculated [CuCu]$^+$ structures and comparison of harmonic spectra with the N_2-tagged spectrum: Distinguishing isomers with IR-IR photobleaching

Our DFT calculations recovered three low lying isomers of **[CuCu]**$^+$ with the structures indicated in Figure 3. Interestingly, the lowest energy structure occurs in the side-on motif, whereas the ebHf form assigned by inspection is calculated to occur 1 kJ/mol higher in energy, followed by the related ebHb isomer 5 kJ/mol above the minimum energy side-on structure. Figure 4 presents the comparison between the calculated spectra with the observed N_2 tagged spectrum in the top trace. An overview of all relevant calculated vibration modes and experimental observed bands are provided in Table 1 The predicted bands for the ebHf isomer are indeed in good agreement with the locations of the bands assigned by the empirical trends. In contrast, the spectrum of the side-on isomer is dramatically different in both the C=O pattern in the fingerprint region and the location of the OH stretch. Specifically, the acid C=O and asymmetric CO stretch of the $-CO_2^-$ group are predicted to come closer together at 1700 and 1800 cm^{-1} where there is very little activity in the observed spectrum. The predicted OH stretch is also ~150 cm^{-1} below the weaker feature (C2) in the experimental spectrum. We therefore conclude that the side-on isomer is not formed in the **[CuCu]**$^+$ complex under the conditions of our ESI ion source.

The calculated patterns provide a compelling assignment of the C2 band to the ebHb rotamer of the end-on bound ebHf dominant form. We verified that this band was indeed due to a distinct species using two-color, IR-IR photobleaching as indicated in the insert in Figure 2D. In that method, negative-going peaks appear according to the removal of population of an isomer by photodissociating it by strong excitation of one of its characteristic transitions. Therefore, the fact that the two peaks C1 and C2 can be selectively removed establishes that they are due to different isomers, and also confirms that they do not interconvert on the microsecond timescale of the pump-probe experiment. The calculated free OH fundamental of the

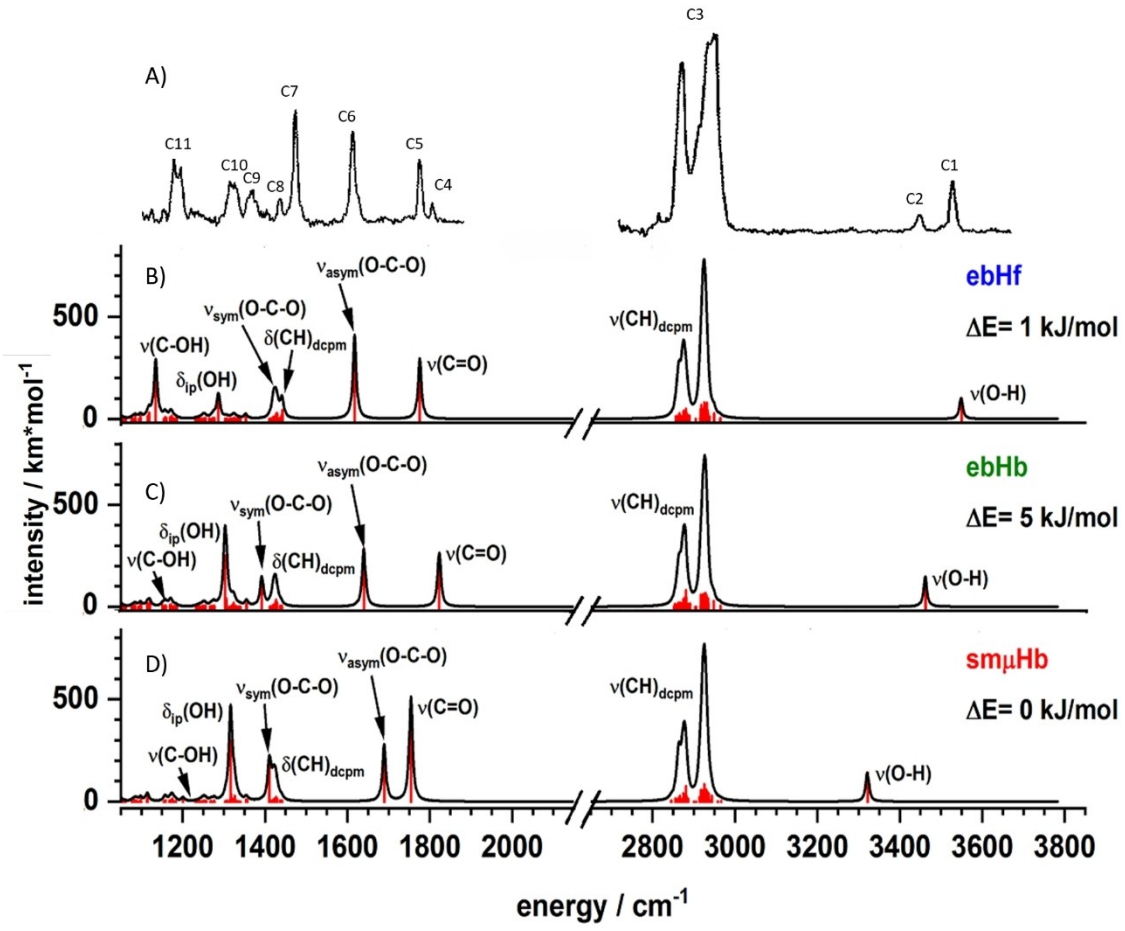

Figure 4. Comparison of the experimental **[CuCu]$^+$** spectrum with those calculated for the three lowest energy isomers recovered in DFT calculations shown in Figure 3. The calculated stick spectra (red) are convoluted with a Lorentzian curve (black, fwhm = 10 cm^{-1}). Level of theory: PBE0/def2TZVP; frequency scaled: 0.961 (900–2200 cm^{-1}), 0.946 (2600–3800 cm^{-1}).

Table 1. Vibrations in **[CuCu]$^+$** by calculations and experiments, DFT frequencies scaled: 0.961 (900-2200 cm^{-1}); 0.946 (2600-3800 cm^{-1}) PBE0/def2TZVP.

Motif	smμHb [ν/cm^{-1}]	ebHb [ν/cm^{-1}]	ebHf [ν/cm^{-1}]	IR-MPD [ν/cm^{-1}]	tagIR-PD [ν/cm^{-1}]
$\delta(CH)_{dcpm}$	985	985	985	–	1010 C12
ν(C–OH)	1220[c–e]	1151[c–e]	1135[c–e]	–	1136/1154 C11
δ_{ip}(OH) (ip: in plane)	1317[c–f]	1303[c,d,f]	1287[c,d,f]	1270-1370 c_5	1288 C9 1343 C10
$\delta(CH)_{dcpm}$	1427	1425	1424	1370-1460 c_4	1452 C7
ν_{sym}(O–C–O)	1411[c–f]	1393[d–f]	1442[d–f]	1370-1460 c_4	1415 C8
ν_{asym}(O–C–O)	1690[d,e]	1640[d,e]	1617[d,e]	1610-1790 c_3	1604 C6
ν(C=O)	1754[b,e]	1823[c,e]	1775[c,e]	1610-1790 c_3	1778 C5 1811 C4
$\nu(C–H)_{dcpm}$	2877/2925	2877/2924	2877/2924	2864/2949 c_2	2861/2939 C3
ν(OH)	3322	3461	3549	3550 c_1	3467 C2 3551 C1

With minor contributions of [a] C=O stretch, [b] asym OCO stretching, [c] sym OCO stretching, [d] CH bending dcpm, [e] OH bending in plane, [f] C-O(-H) stretch.

ebHb isomer (3461 cm^{-1}) is in excellent agreement with the observed C2 band (3467 cm^{-1}). The subtle reorientation of the OH group is not predicted to have a strong effect on the C=O stretches of the scaffold, thus accounting for the relatively simple N_2-tagged spectrum despite the fact that it represents contributions from two isomers. The specific transitions asso-

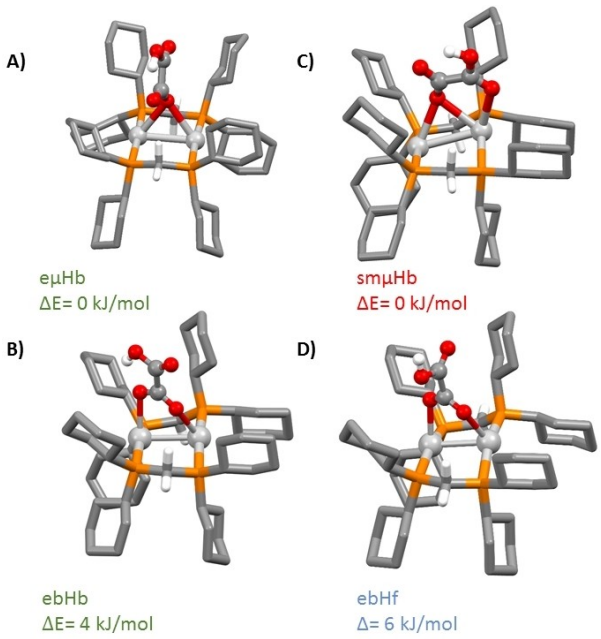

Figure 5. Calculated low-lying structures of **[AgAg]$^+$**. Atoms are coded by color (silver for Ag, orange for P, red for O, grey for C, white for H); isomers are coded for their structures as follows: e: end-on, s: side-on, b: bidentate, m: monodentate, μ: one O-atom coordinates between two metal atoms, Hf: free OH, Hb: bonded OH. For a better overview, H atoms of cyclohexyl group are omitted. Relative energies are given for each isomer. More isomers are shown in Figure S1. Level of theory: PBE0/def2TZVP.

ciated with each isomer were quantified applying the two-color photobleaching method. This was carried out by modulating the populations of the ebHf and ebHb isomers by fixing the bleaching laser on the C1 and C2 transitions, respectively, and monitoring the probe response on the various bands in the fingerprint region. The results of these measurements are presented in Figure S2 in the Supporting Information, and indeed the strong bands C4-C7 are common to both isomers.

Calculated [AgAg]$^+$ structures and comparison of harmonic spectra with the N_2-tagged spectrum: Distinguishing isomers with IR-IR photobleaching

The persistence of the band pattern displayed by **[CuCu]$^+$** in the **[AgAg]$^+$** spectrum (Figure 2C) strongly suggests that the ebHf and ebHb isomeric types adopted by **[CuCu]$^+$** are also present in **[AgAg]$^+$**. On the other hand, the new bands present in the **[AgAg]$^+$** spectrum fall in the general regions expected for the side-on attachment. In particular, **[AgAg]$^+$** displays a very red-shifted, broader feature lowest in the OH stretching region (A3), along with an interloper feature (* in Figure 2C at 1664 cm^{-1}) close to the frequency of the $\nu_{asym}^{(O-C-O)}$ stretch calculated for the smμHb **[CuCu]$^+$** isomer. The four lowest energy structures recovered by DFT calculations for **[AgAg]$^+$** are included in Figure 5. An overview of all relevant calculated vibration modes and experimental observed bands are provided in Table 2 Both side-on and end-on forms are again predicted to be available but note that the end-on form also has distorted arrangement, eμHb (Figure 5A), in which one of the $-CO_2^-$ oxygen atoms binds preferentially to both metal centers.

Figure 6 presents a comparison of the N_2-tagged **[AgAg]$^+$** spectrum with the calculated spectra for three of the four isomers (smμHb, ebHf, and eμHb) indicated in Figure 5. It is immediately clear that the interloper (A7, *) discussed above at 1664 cm^{-1} is accurately predicted to be the $\nu_{asym}^{(O-C-O)}$ stretch of the side-on (smμHb) isomer (Figure 6B), which also accounts for the most red shifted feature (A3) in the OH stretching region. The higher frequency bands (A1 and A2) are predicted for the OH stretches of the end-on forms (eμHb and ebHf) with calculated spectra in Figure 6D and 6F, respectively.

Table 2. Vibrations in **[AgAg]$^+$** by calculations and experiments, DFT frequencies scaled: 0.961 (900-2200 cm^{-1}); 0.946 (2600-3800 cm^{-1}) PBE0/def2TZVP.

Motif	smμHb [ν/cm^{-1}]	ebHb [ν/cm^{-1}]	eμHb [ν/cm^{-1}]	ebHf [ν/cm^{-1}]	IR-MPD [ν/cm^{-1}]	tagIR-PD [ν/cm^{-1}]
$\delta(CH)_{dcpm}$	984	984	984	984	–	1001 A16
ν(C–OH)	1191[c–e]	1149[c–e]	1169[c–e]	1129[c–e]	–	1145 A15
δ_{ip}(OH) (ip: in plane)	1324[c,d,f]	1313[c,d,f]	1317[c,d,f]	1280[c,d,f]	1273 a_9	1283 A14
					1317 a_8	1307 A13
					1352 a_7	1331 A12
$\delta(CH)_{dcpm}$	1423	1424	1424	1428	1453 a_4	1451 A10
ν_{sym}(O–C–O)	1404[d–f]	1381[d–f]	1393[d–f]	1421[d–f]	1412 a_6	1402 A11
					1434 a_5	1410 A11
ν_{asym}(O–C–O)	1673[d,e]	1636[d,e]	1642[d,e]	1613[d,e]	1610-1790 a_3	1592 A9
						1616 A8
						1664 A7
ν(C=O)	1756[c,e]	1816[c,e]	1790[c,e]	1770[c,e]	1610-1790 a_3	1749 A6
						1805 A5
$\nu(C–H)_{dcpm}$	2876/2925	2876/2926	2877/2926	2875/2925	2866/2952 a_2	2866/2929/2947 A4
ν(OH)	3248	3404	3351	3549	3550 a_1	3161 A3
						3416 A2
						3551 A1

With minor contributions of [a] C=O stretch, [b] asym OCO stretching, [c] sym OCO stretching, [d] CH bending dcpm, [e] OH bending in plane, [f] C-O(-H) stretch.

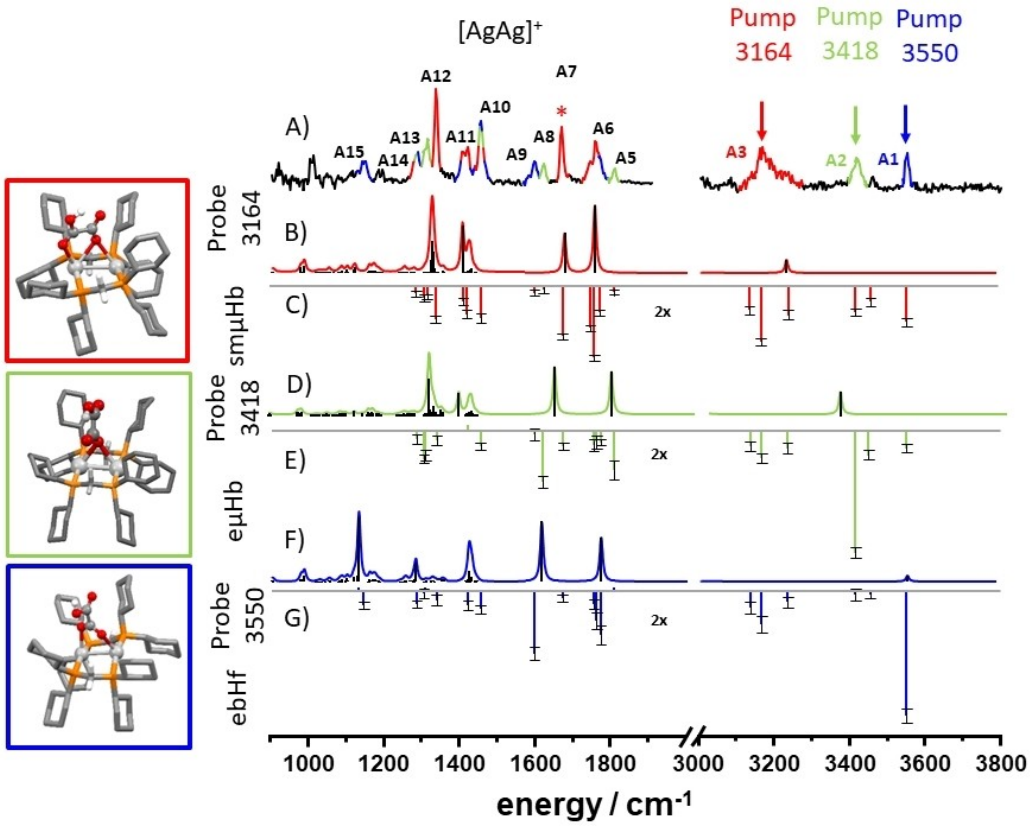

Figure 6. (A) IR-PD spectrum of N_2-tagged **[AgAg]$^+$** at 40 K, (C, E, G) fixed-frequency photobleaching experiments probing 3164, 3418, 3550 cm^{-1} bands A3-1, respectively. Downward lines indicate the degree of population modulation of the various bands when the A1, A2 and A3 bands are bleached by the pump laser. (B, D, F) calculated IR absorption spectra of isomer smμHb (red), eμHb (green), and ebHf (blue), respectively. The stick spectra (black) are convoluted with a Lorentzian curve (fwhm = 10 cm^{-1}). Level of theory: PBE0/def2TZVP; frequency scaled: 0.961 (900–2200 cm^{-1}), 0.946 (2600–3800 cm^{-1}).

Although the calculated spectra provide compelling assignments for the observed bands in the context of three isomer classes (smμHb, eμHb, and ebHf), this scheme can be tested experimentally using the isomer-selective, two color IR-IR photobleaching scheme that was used to establish the presence of two isomers in the **[CuCu]$^+$** spectrum. The downward lines in Figure 6C, 6E and 6F correspond to the degree of population modulation driven by the pump set on the A3 (red), A2 (green) and A1 (blue) free OH features, respectively. Interestingly, photobleaching the two highest energy OH bands (A1 and A2) yield mutually exclusive population removal, thus establishing that these features are indeed due to two non-interconverting isomers. They also account for closely spaced bands around 1600 and 1800 cm^{-1} that are predicted for the end-on rotamers ebHf and eμHb, similar to the situation encountered in the **[CuCu]$^+$** system. In particular, the A5 feature is uniquely modulated by bleaching at the A2 band, consistent with the calculated blue shift in its C=O stretching band, clearly relating both bands to the eμHb isomer. Note that the A7/(*) band is not associated with these end-on isomers. We therefore conclude that the eμHb and ebHf forms are adopted by the **[AgAg]$^+$** complex.

Photobleaching at A3 band also depletes the population in the A7 feature as shown in Figure 6C, consistent with its assignment to the side-on isomer smμHb. Surprisingly, however, we note that photobleaching the A1 and A2 bands also partially depletes the population contributing to the A3 feature (Figures 6E and 6G) and bleaching A3 yields depletion across the entire spectrum as indicated in trace C of Figure 6! The fact that the isomers yielding bands A1 and A2 show little to no interconversion, while bleaching either one also depletes the population responsible for band A3, may be understood if the broad A3 feature results from some isomerization of smμHb to eμHb or ebHf, or vica versa.

Summarizing, two-color IR-IR photobleaching experiments reveal three distinct spectral patterns in the N_2-tagged **[AgAg]$^+$** spectrum. These patterns are consistent with the formation of both end-on and side-on docking motifs. The end-on forms correspond to the OH rotamers, and the blue-shift of the C=O stretch in the isomer with a bound OH indicates that it likely occurs with the asymmetric eμHb attachment to the two Ag^+ ions. The side-on form (smμHb) is clearly present as evidenced by a characteristic $\nu_{asym}^{(O-C-O)}$ stretching fundamental at 1664 cm^{-1}, and it is at least partially responsible for the red-shifted broad feature in the OH stretching region near 3250 cm^{-1}. Our DFT modelling of likely isomerization barriers (Section S5, Figures S11-13, Tables S4–S5 in the Supporting Information) identified likely pathways that may connect the

identified isomers of **[CuCu]**$^+$ and **[AgAg]**$^+$ while the predicted barrier heights are subject of discussion and reveal no clear correlation with the experimental findings.

Interrogating the complex structure at 300 K with IR-MPD, CID and ion-mobility

300 Kelvin IR-MPD spectra of **[CuCu]**$^+$ and **[AgAg]**$^+$ are compared with the N_2-tagged spectra in Figure 7. Although the behavior of the CH stretching bands is very similar in both complexes, the IR-MPD spectra only display OH stretching bands in accord with free OH isomers (A1/a_1 and C1/c_1); the H-bonded features that appear lower in energy in the tagged spectra are missing. More interestingly, the IR-MPD bands in the fingerprint region are significantly broadened with respect to those from the tagged ions. This suggests that the HOx substrates are labile such that many configurations are available, or are interconverting such that the C=O stretching frequencies are fluctuating as different binding motifs are adopted.

Given the fact that both **[CuCu]**$^+$ and **[AgAg]**$^+$ display diffuse IR bands at 300 K, it is useful to explore whether there are chemical differences that survive even when interconversion is likely taking place. This issue was addressed by comparing the (300 K) CID fragmentation pathways of the two complexes. **[CuCu]**$^+$ complexes fragment by preferential dcpm ligand loss with some oxalic acid (H_2Ox or XH) formation or dcpm + [C_2O_3] loss to lesser extent. The **[AgAg]**$^+$ complex, on the other hand, displays a strong preference for H_2Ox formation (Figure S8) These findings are much in line with the cryo hole burning experiments, and reinforce "chemical intuition" such as the HSAB principle,[21] which posits that Cu and Ag are harder and softer cations by direct comparison, resulting in strong and weak binding to "hard" HOx, respectively. The observed weaker binding supports the increased number of **[AgAg]**$^+$ isomers seen here. For further details, refer to Section S3 in the Supporting Information.

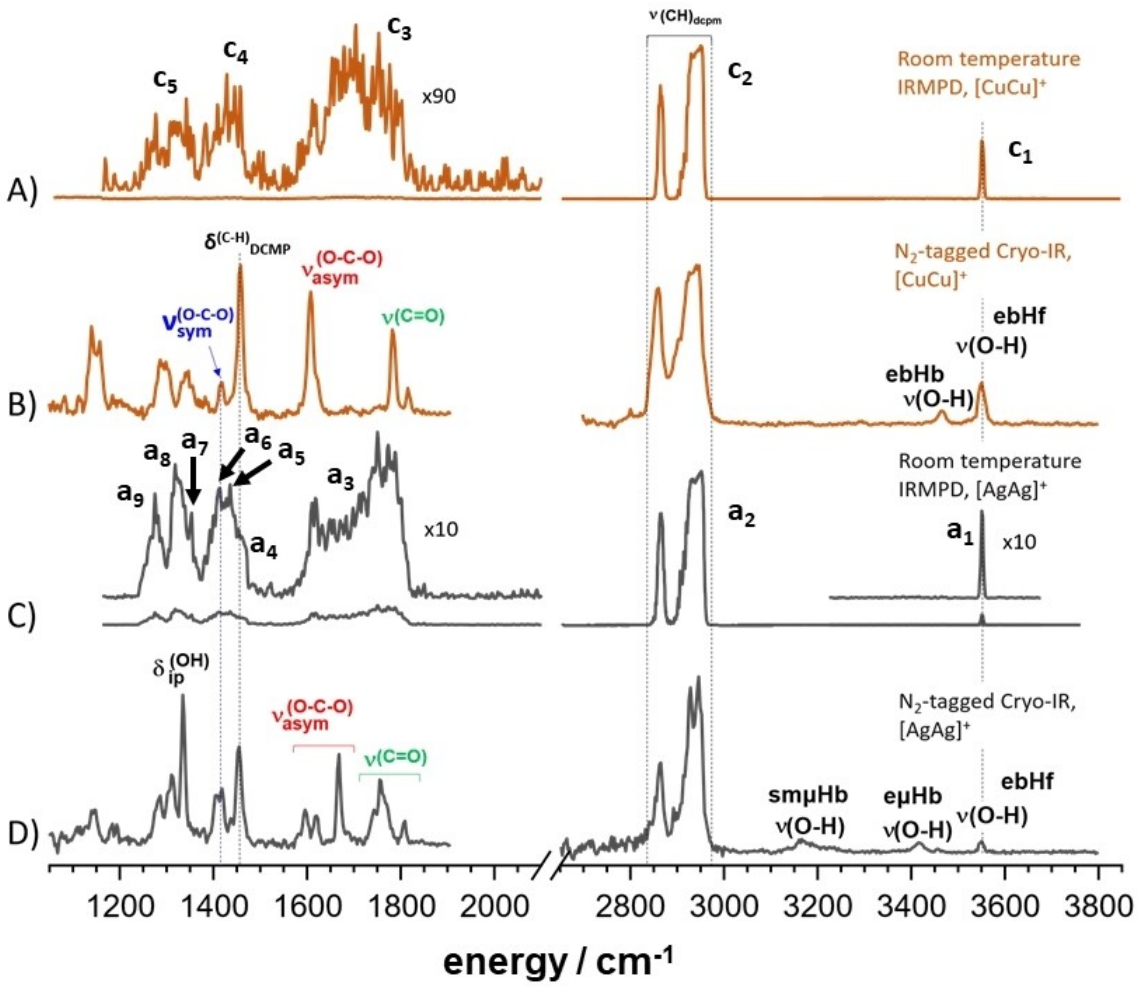

Figure 7. (a) IR-MPD spectrum of **[CuCu]**$^+$ at 300 K, (b) IR-PD spectrum of N_2-tagged **[CuCu]**$^+$ at 40 K, (c) IR-MPD spectrum of **[AgAg]**$^+$ at 300 K (d) IR-PD spectrum of N_2-tagged **[AgAg]**$^+$ at 40 K. Weak IR-MPD features of (a) and (c) in the range of 1200–2000 cm^{-1} are enhanced by factors of 10 and 90, respectively.

Finally, we investigated the possibility that the 300 K complexes exhibit different spatial cross sections, perhaps reflecting the large amplitude motions of the substrates in different binding regimes. Unfortunately, ion mobility studies of $[\mathbf{CuCu}]^+$ and $[\mathbf{AgAg}]^+$ complexes could not differentiate distinguishable isomers. Either the cross sections of coexisting isomers are most similar, or they are interconverting on the ms time scales of the experiments. For further details, refer to the Supporting Information (Section S4, Figure S10).

Conclusion and Outlook

This study characterizes the dynamic bonding of hydrogen oxalate HOx to phosphine stabilized $[\mathbf{CuCu}]^+$ and $[\mathbf{AgAg}]^+$ complexes in isolation, and it finds evidence for two HOx binding isomers of $[\mathbf{CuCu}]^+$ and for three isomers of $[\mathbf{AgAg}]^+$. Cryo tagging IR-PD spectra elucidate the isomerism of $[\mathbf{CuCu}]^+$ and $[\mathbf{AgAg}]^+$, and the modelling of these spectra by DFT helps to assign likely isomers. Two colour bleach-probe IR-IR hole burning experiments confirm the tentative assignments of most bands, and they indicate some minor amount of isomeric interconversions in $[\mathbf{AgAg}]^+$ - as opposed to $[\mathbf{CuCu}]^+$ where stiff HOx coordination clearly suppresses such conversions. Room temperature IR-MPD spectra confirm free OH isomers and lack evidence for hydrogen bonded OH isomers. The DFT modelling supports isomeric assignments and the analysis of vibrational spectra. It correlates IR-PD and IR-MPD bands to possible HOx binding motifs. The collision induced dissociation studies reveal competing fragmentation channels in the case of $[\mathbf{CuCu}]^+$ and a dominating H_2Ox loss in the case of $[\mathbf{AgAg}]^+$ which points towards strong HOx bonding in $[\mathbf{CuCu}]^+$ and weaker HOx bonding in $[\mathbf{AgAg}]^+$. The DFT modelling fails, however, to predict transition states which would explain the observed absence and occurrence of isomeric interconversions in $[\mathbf{CuCu}]^+$ and $[\mathbf{AgAg}]^+$, respectively. Ion mobility studies confirm that isomers of $[\mathbf{CuCu}]^+$ and $[\mathbf{AgAg}]^+$ if any must be very similar of swiftly interconverting.

It is obviously valuable to continue and extend this multi-method approach order to achieve the most complete understanding of the reaction pathways available to small molecule substrates bound to dinuclear coordination compounds. A strong motivation for such fundamental information is that this class of systems provide promising templates for [CO_2, H_2] capture and storage.

Acknowledgements

This work was supported by the state research center OPTIMAS and by the German research foundation DFG within the transregional collaborative research center SFB/TRR 88 "Cooperative effects in homo and heterometallic complexes" (3MET.de, project C4, C6 and project A5). The N_2-tagging and isomer-selective spectra presented in this work was supported by the Air Force Office of Scientific Research under AFOSR Award No. FA9550-18-1-0213 (M.J.). Open Access funding enabled and organized by Projekt DEAL.

Conflict of Interest

The authors declare no conflict of interest.

Keywords: coinage metals · hydrogen oxalate · IR spectroscopy · isomers · pump probe spectroscopy

[1] a) D. McNevin, S. von Caemmerer, G. Farquhar, *J. Exp. Bot.* **2006**, *57*, 3883–3900; b) W. A. Laing, J. T. Christeller, *Biochem. J.* **1976**, *159*, 563–570; c) F. J. Millero, *Geochim. Cosmochim. Acta* **1995**, *59*, 661–677.
[2] R. Angamuthu, P. Byers, M. Lutz, A. L. Spek, E. Bouwman, *Science* **2010**, *327*, 313–315.
[3] J. Lan, T. Liao, T. Zhang, L. W. Chung, *Inorg. Chem.* **2017**, *56*, 6809–6819.
[4] a) A. T. Royappa, A. D. Royappa, R. F. Moral, A. L. Rheingold, R. J. Papoular, D. M. Blum, T. Q. Duong, J. R. Stepherson, O. D. Vu, B. Chen, M. R. Suchomel, J. A. Golen, G. André, N. Kourkoumelis, A. D. Mercer, A. M. Pekarek, D. C. Kelly, *Polyhedron* **2016**, *119*, 563–574; b) K. Köhler, J. Eichhorn, F. Meyer, D. Vidovic, *Organometallics* **2003**, *22*, 4426–4432; c) A. Jakob, H. Schmidt, P. Djiele, Y. Shen, H. Lang, *Microchim. Acta* **2006**, *156*, 77–81; d) A. Jakob, T. Rüffer, P. Ecorchard, B. Walfort, K. Körbitz, S. Frühauf, S. E. Schulz, T. Gessner, H. Lang, *Z. Anorg. Allg. Chem.* **2010**, *636*, 1931–1940; e) T. Haase, K. Kohse-Höinghaus, N. Bahlawane, P. Djiele, A. Jakob, H. Lang, *Chem. Vap. Deposition* **2005**, *11*, 195–205.
[5] a) H. Schwarz, K. R. Asmis, *Chem. Eur. J.* **2019**, *25*, 2112–2126; b) M. A. Duncan, *J. Phys. Chem. A* **2012**, *116*, 11477–11491; c) H. Schwarz, *Coord. Chem. Rev.* **2017**, *334*, 112–123; d) A. J. Ingram, A. B. Wolk, C. Flender, J. Zhang, C. J. Johnson, U. Hintermair, R. H. Crabtree, M. A. Johnson, R. N. Zare, *Inorg. Chem.* **2014**, *53*, 423–433; e) E. Garand, J. A. Fournier, M. Z. Kamrath, N. D. Schley, R. H. Crabtree, M. A. Johnson, *Phys. Chem. Chem. Phys.* **2012**, *14*, 10109–10113; f) F. S. Menges, S. M. Craig, N. Totsch, A. Bloomfield, S. Ghosh, H. J. Kruger, M. A. Johnson, *Angew. Chem. Int. Ed.* **2016**, *55*, 1282–1285; *Angew. Chem.* **2016**, *128*, 1304–1307.
[6] V. W.-W. Yam, V. K.-M. Au, S. Y.-L. Leung, *Chem. Rev.* **2015**, *115*, 7589–7728.
[7] a) R. A. J. O'Hair, N. J. Rijs, *Acc. Chem. Res.* **2015**, *48*, 329–340; b) A. Zavras, G. N. Khairallah, M. Krstić, M. Girod, S. Daly, R. Antoine, P. Maitre, R. J. Mulder, S.-A. Alexander, V. Bonačić-Koutecký, P. Dugourd, R. A. J. O'Hair, *Nat. Commun.* **2016**, *7*, 11746; c) A. Zavras, M. Krstić, P. Dugourd, V. Bonačić-Koutecký, R. A. J. O'Hair, *ChemCatChem* **2017**, *9*, 1298–1302.
[8] a) S. V. Kruppa, F. Bäppler, W. Klopper, S. P. Walg, W. R. Thiel, R. Diller, C. Riehn, *Phys. Chem. Chem. Phys.* **2017**, *19*, 22785–22800; b) S. V. Kruppa, F. Bäppler, C. Holzer, W. Klopper, R. Diller, C. Riehn, *J. Phys. Chem. Lett.* **2018**, *9*, 804–810; c) S. V. Kruppa, C. Gross, X. Gui, F. Bappler, B. Kwasigroch, Y. Sun, R. Diller, W. Klopper, G. Niedner-Schatteburg, C. Riehn, W. R. Thiel, *Chem. Eur. J.* **2019**, *25*, 11269–11284.
[9] D. Li, C.-M. Che, H.-L. Kwong, V. W.-W. Yam, *J. Chem. Soc. Dalton Trans.* **1992**, 3325–3329.
[10] C.-M. Che, M.-C. Tse, M. C. W. Chan, K.-K. Cheung, D. L. Phillips, K.-H. Leung, *J. Am. Chem. Soc.* **2000**, *122*, 2464–2468.
[11] a) P. K. Mehrotra, R. Hoffmann, *Inorg. Chem.* **1978**, *17*, 2187–2189; b) H. Schmidbaur, A. Schier, *Angew. Chem. Int. Ed.* **2015**, *54*, 746–784; *Angew. Chem.* **2015**, *127*, 756–797; c) M. Jansen, *Angew. Chem. Int. Ed.* **1987**, *26*, 1098–1110; *Angew. Chem.* **1987**, *99*, 1136–1149.
[12] a) J. K. Denton, P. J. Kelleher, M. A. Johnson, M. D. Baer, S. M. Kathmann, C. J. Mundy, B. A. Wellen Rudd, H. C. Allen, T. H. Choi, K. D. Jordan, *Proc. Natl. Acad. Sci. USA* **2019**, *116*, 14874–14880; b) J. W. DePalma, P. J. Kelleher, L. C. Tavares, M. A. Johnson, *J. Phys. Chem. Lett.* **2017**, *8*, 484–488.
[13] a) C. H. Duong, N. Yang, P. J. Kelleher, M. A. Johnson, R. J. DiRisio, A. B. McCoy, Q. Yu, J. M. Bowman, B. V. Henderson, K. D. Jordan, *J. Phys. Chem. A* **2018**, *122*, 9275–9284; b) N. Yang, C. H. Duong, P. J. Kelleher, A. B. McCoy, M. A. Johnson, *Science* **2019**, *364*, 275–278.
[14] Y. Nosenko, F. Menges, C. Riehn, G. Niedner-Schatteburg, *Phys. Chem. Chem. Phys.* **2013**, *15*, 8171–8178.
[15] a) C. Adamo, V. Barone, *J. Phys. Chem. Lett.* **1999**, *110*, 6158–6170; b) F. Weigend, R. Ahlrichs, *Phys. Chem. Chem. Phys.* **2005**, *7*, 3297–3305.

[16] Gaussian 16, Revision C.01, M. J. Frisch, G. W. Trucks, H. B. Schlegel, G. E. Scuseria, M. A. Robb, J. R. Cheeseman, G. Scalmani, V. Barone, G. A. Petersson, H. Nakatsuji, X. Li, M. Caricato, A. V. Marenich, J. Bloino, B. G. Janesko, R. Gomperts, B. Mennucci, H. P. Hratchian, J. V. Ortiz, A. F. Izmaylov, J. L. Sonnenberg, Williams, F. Ding, F. Lipparini, F. Egidi, J. Goings, B. Peng, A. Petrone, T. Henderson, D. Ranasinghe, V. G. Zakrzewski, J. Gao, N. Rega, G. Zheng, W. Liang, M. Hada, M. Ehara, K. Toyota, R. Fukuda, J. Hasegawa, M. Ishida, T. Nakajima, Y. Honda, O. Kitao, H. Nakai, T. Vreven, K. Throssell, J. A. Montgomery Jr., J. E. Peralta, F. Ogliaro, M. J. Bearpark, J. J. Heyd, E. N. Brothers, K. N. Kudin, V. N. Staroverov, T. A. Keith, R. Kobayashi, J. Normand, K. Raghavachari, A. P. Rendell, J. C. Burant, S. S. Iyengar, J. Tomasi, M. Cossi, J. M. Millam, M. Klene, C. Adamo, R. Cammi, J. W. Ochterski, R. L. Martin, K. Morokuma, O. Farkas, J. B. Foresman, D. J. Fox, Gaussian Inc., Wallingford, CT, **2016**.
[17] C. Peng, H. B. Schlegel, *Isr. J. Chem.* **1993**, *33*, 449–454.
[18] S. Sklenak, J. Hrusak, *J. Chem. Theory Comput.* **2006**, *2*, 997–1008.
[19] C. T. Wolke, A. F. DeBlase, C. M. Leavitt, A. B. McCoy, M. A. Johnson, *J. Phys. Chem. A* **2015**, *119*, 13018–13024.
[20] a) C. M. Leavitt, A. B. Wolk, M. Z. Kamrath, E. Garand, M. J. Van Stipdonk, M. A. Johnson, *J. Am. Soc. Mass Spectrom.* **2011**, *22*, 1941–1952; b) T. Khuu, N. Yang, M. A. Johnson, *Int. J. Mass Spectrom.* **2020**, *457*, 116427.
[21] R. G. Pearson, *J. Am. Chem. Soc.* **1963**, *85*, 3533–3539.

Manuscript received: July 30, 2021
Accepted manuscript online: October 10, 2021
Version of record online: October 27, 2021

